Butwal Campus Journal, Vol. 8, No. 1: 57-71, August 2025
Research Management Cell, Butwal Multiple Campus, Tribhuvan University, Nepal
DOI: https://doi.org/10.3126/bcj.v8i1.85493

First-Principles Insight into the Structural and Electronic Properties of Metronidazole and Tinidazole

Sagar Sharma[1], Kamal Khanal [1,2*]
1 Department of Physics, Butwal Multiple Campus, Tribhuvan University, Butwal, Nepal
2 Central Department of Physics, Tribhuvan University, Kirtipur, Kathmandu
*****Corresponding author email: kamal.khanal@bumc.tu.edu.np

Abstract

Metronidazole and tinidazole are among the most significant nitroimidazole antibiotics, essential for treating anaerobic bacterial and protozoal infections. These two drugs were studied using DFT at the B3LYP/6-31 G (d,p) level, as implemented in Gaussian 16W, for all major quantum mechanical calculations. Tinidazole (E_{gap} = 4.60 eV) was found to be somewhat more stable than metronidazole (E_{gap} = 4.58 eV), with a small difference in their energy gap. The DOS spectra validated the results of FMO analysis. Tinidazole, with a slightly higher electrophilicity of 5.07 eV compared to metronidazole's 4.86 eV, was observed to be a stronger electrophile. The Mulliken atomic charges and MEP surface analysis explained the difference in charge distribution and attack sites due to structural differences. The UV-Vis absorption spectra showed stronger absorption intensity in tinidazole compared to metronidazole, even though both exhibit similar spectral patterns, which is due to the presence of the ethylsulphonylethyl side chain in tinidazole. The FT-Raman spectra were almost similar for both drugs, while we observed some higher peaks in tinidazole than in metronidazole in the FT-IR spectra. The NCI-RDG analysis showed stronger van der Waals interactions and stronger steric repulsive effects in tinidazole than in metronidazole.

Keywords: DFT, metronidazole, tinidazole, MEP, NCI-RDG.

Introduction

Nitroimidazole antibiotics are considered to be a crucial class of antimicrobial agents used to treat anaerobic bacterial and protozoal infections (Mital, 2009). These compounds become activated under low oxygen conditions, where their nitro groups undergo reduction to generate reactive radicals that disrupt microbial DNA (Jenks, 2010). Metronidazole and tinidazole are two prominent drugs in this class. Metronidazole, developed and commercialized in 1960 (Corey, 2013), is mainly utilized for treating various anaerobic infections like bacterial vaginosis, trichomoniasis, giardiasis, amoebiasis, and clostridiasis (Schwebke and Desmond, 2011). On the other hand, tinidazole, developed in 1972, shares the same nitroimidazole core but is differentiated by the ethylsulphonylethyl side chain (Ebel et al., 2002). Despite these structural similarities, these drugs show notable physicochemical differences.

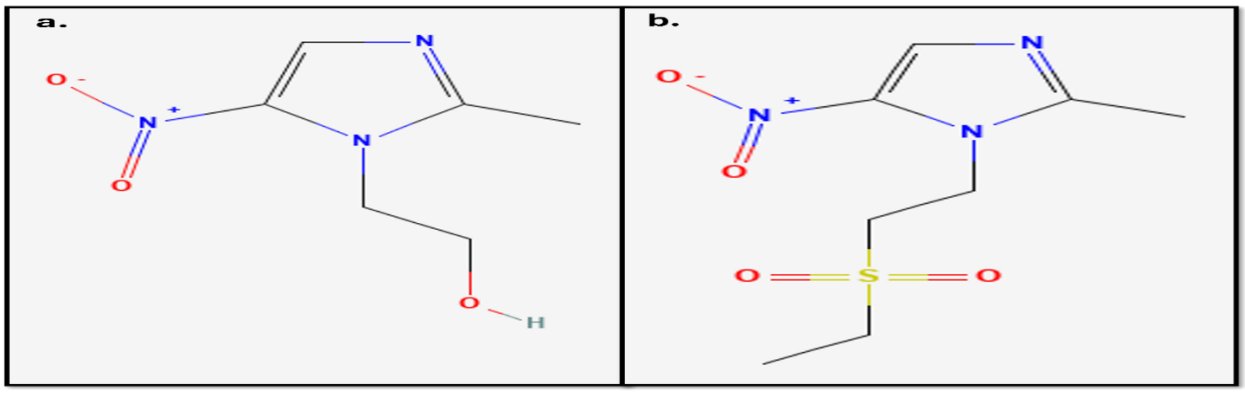

Figure 1: Chemical structure of (a) metronidazole (CID: 4173) and (b) tinidazole (CID: 5479) (PubChem Database)

Density Functional Theory (DFT) has been considered a powerful tool for getting insights into the electronic structure, reactivity, stability, and spectroscopic behavior of various pharmaceutical compounds. DFT study on nitro-containing compounds revealed the electron-donating and withdrawing groups that influence different degradation pathways (He et al., 2021). Another similar study conducted theoretical spectroscopic analysis, especially Raman bands, for the identification of compounds (Shi et al., 2022). The impact of biofield treatment on two drugs, metronidazole and tinidazole, was studied based on FT-IR and UV-Vis spectroscopy (Trivedi et al., 2015). The efficacy of these two drugs was compared to determine the best out of them for the treatment of bacterial vaginosis (Schwebke and Desmond, 2011). However, until now, there has been no systematic study that compared metronidazole and tinidazole at the quantum level. So, bridging this gap can improve our understanding of how the structural differences of these two drugs influence their physicochemical and pharmacokinetic properties.

Methodology

The initial coordinates for metronidazole and tinidazole were obtained from the PubChem Database as PubChem CID: 4173 for metronidazole and PubChem CID: 5479 for tinidazole. Density Functional Theory (DFT) calculations were conducted utilizing the Gaussian 16W software package (Frisch et al., 2016). Geometry optimizations and energy calculations were performed on the metronidazole, tinidazole utilizing the B3LYP hybrid functional in integration with the 6-31G(d,p) basis set in the Gaussian 16W program. The B3LYP functional was selected because of its proven reliability and computational efficiency in modeling materials (Becke, 1993; Lee et al., 1988). The density of states spectra (DOS) of metronidazole, tinidazole were computed adopting the GaussSum 3.0 program (O'boyle et al., 2008). Various global reactivity descriptors were also examined at the B3LYP/6-31G(d,p) level. Additionally, Time-Dependent DFT (TD-DFT), available in Gaussian 16W, was employed to simulate the UV–Visible absorption spectra (Casida, 2009). Visualization and analysis of molecular orbitals, charge distributions, and spectra were performed using GaussView 6.0 (Dennington et al., 2016). Furthermore, Molecular Electrostatic Potential (MEP)

mapping and Mulliken charge distribution analyses were conducted to assess charge localization and identify potential interaction sites within the materials (Mulliken, 1955). NCI-RDG analysis was conducted using Multiwfn (Lu and Chen, 2012) and VMD software (Humphrey et al., 1996). Koopmans theorem (Koopmans, 1934) was used for determining the energy gap given by the LUMO and HOMO, which gives rise to several other quantum chemical descriptors including Ionization Potential (IP), Electron Affinity (EA), Electronegativity (χ), Chemical potential (μ), Chemical hardness (η), Chemical softness (S) and the Electrophilicity Index (ω) (Padmanabhan et al., 2007; Pearson, 1989; Geerlings et al., 2003).

Results and Discussions

Optimized Geometry

Two title compounds under study, metronidazole and tinidazole, were optimized at their minimum energy configurations, which is validated by the presence of zero negative wavenumbers. The global minimum energies of metronidazole and tinidazole were obtained as -623 and -1175 Hartrees, respectively. The optimized geometrical structure of the two drugs, metronidazole and tinidazole, is shown in Figure 2 with symbols and numbering of atoms.

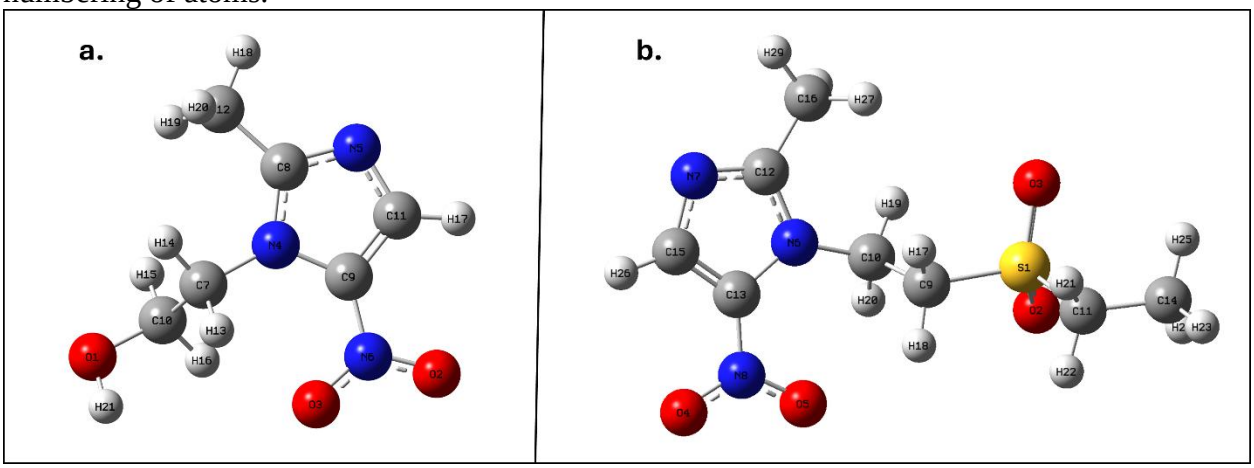

Figure 2: Minimum energy configuration geometry of (a) metronidazole and (b) tinidazole

FMOs (HOMO-LUMO) Study

Frontier Molecular Orbital (FMO) theory is a fundamental framework employed to explain a molecule's reactivity and electronic characteristics. It focuses on two key orbitals: the Highest Occupied Molecular Orbital (HOMO), which reflects the ability of the molecule to donate electrons, while the Lowest Unoccupied Molecular Orbital (LUMO) represents its capacity to accept electrons (Khanal et al., 2025). A key parameter in FMO theory is the HOMO–LUMO energy gap (E_g), which quantifies the energy required to excite an electron from the HOMO to the LUMO. It is calculated using the relation: $E_g = E_{LUMO} - E_{HOMO}$, where E_{HOMO} and E_{LUMO} denote the orbital energies of the HOMO and LUMO, respectively. Typically, HOMO and LUMO are visually represented using two colors: green for the positive phase and red for the

negative phase. A smaller energy gap generally indicates higher chemical reactivity, enhanced polarizability, lower kinetic stability, and vice versa (Adhikari et al., 2024). The HOMO energies of metronidazole and tinidazole are -7.01 eV and -7.13 eV, respectively, whereas the LUMO energies for those drugs are obtained as -2.43 eV and -2.53 eV, resulting in their respective energy gaps as 4.58 eV and 4.60 eV. This smaller difference in their energy gaps indicates that tinidazole is somehow more stable and less reactive compared to metronidazole. In metronidazole, both HOMO and LUMO are localized primarily at the nitroimidazole core, while somewhat in the substituted regions. But, HOMO-LUMO are localized only in the central nitroimidazole core in the case of tinidazole.

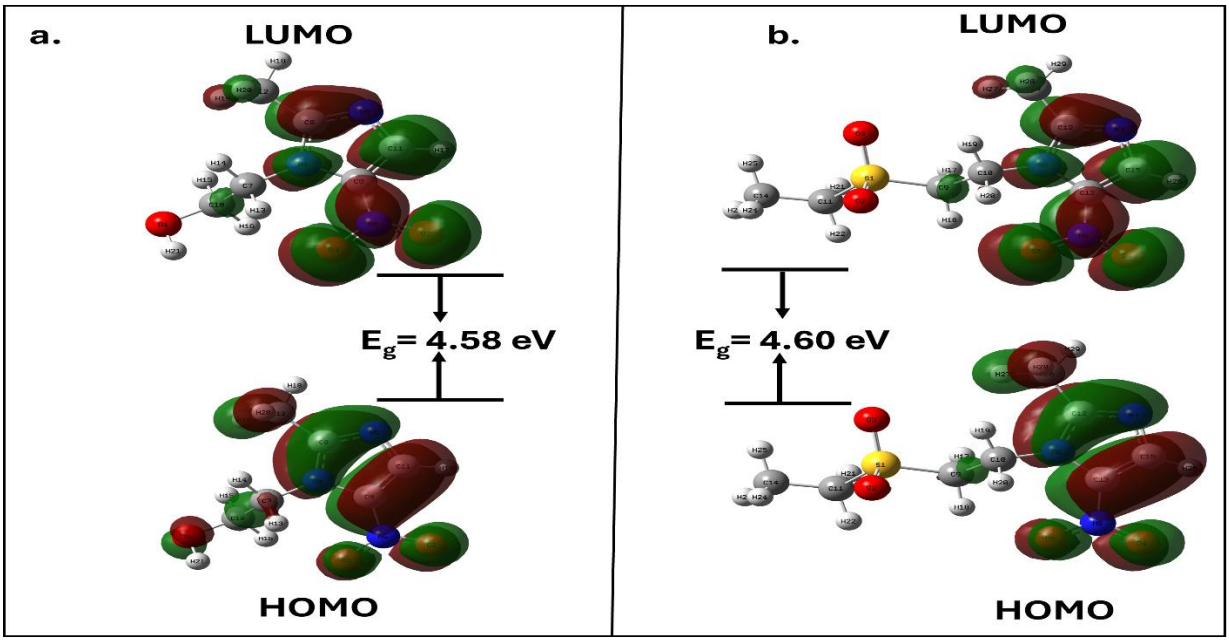

Figure 3: FMOs of (a) metronidazole and (b) tinidazole

Density of States (DOS) Spectra

The density of states spectra (DOS) typically gives the number of energy levels or quantum states occupied per unit increase in energy (Ben Mahmoud et al., 2020; Pandey et al., 2011). Higher spectrum symbolizes more quantum states available for occupancy. The green lines in the DOS spectra denote the HOMO energy levels, while the red lines indicate the LUMO energy levels. The DOS spectra of the title compounds, metronidazole and tinidazole, in the gas phase within the energy level -15eV to +5eV are shown in Figure 4. From the DOS spectra, we observed the energy gap of metronidazole, 4.58eV, and that of tinidazole, 4.60eV, which validates the former FMO study.

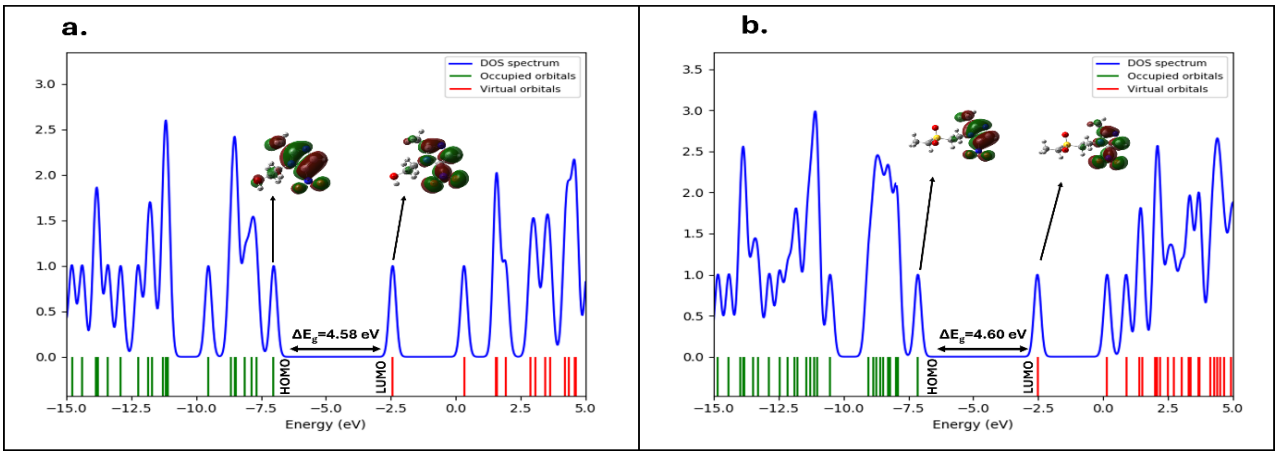

Figure 4: DOS spectra of (a) metronidazole and (b) tinidazole

Global Reactivity Descriptors

The various quantum chemical descriptors listed in Table 1 provide significant insight into the reactivity of the title compounds. The difference in HOMO and LUMO energies gives an energy gap, which was obtained as 4.58 eV for metronidazole and 4.60 eV for tinidazole, suggesting better stability and less reactivity of tinidazole over metronidazole. From the index of Global Electrophilicity (Domingo et al., 2016), the organic compounds can be divided into three types as strong electrophiles having $\omega>1.5$eV, moderate electrophiles with $0.8\text{eV}<\omega>1.5\text{eV}$, and weak electrophiles having $\omega<0.8$eV. From this research, we found that both drugs fall under the category of strong electrophiles, which means they have a higher tendency to accept electrons, with tinidazole being a stronger electrophile than metronidazole. The high ionization potential 7.01 eV and 7.13 eV, and low electron affinity 2.43 eV and 2.53 eV for the drugs metronidazole and tinidazole imply that these molecules are stable and less reactive. Chemical hardness is supposed to be a reliable indicator of the stability of a molecule. Hard molecules are less polarizable than soft ones. The chemical hardness of these molecules is about 3 eV, and softness is low, which means both drugs are chemically hard, symbolizing chemically inert and stable, as well as resistance to charge deformation, making them good candidates for different biological applications like enzyme inhibition. The chemical potential is computed as highly negative for both drugs, which indicates the compounds are thermodynamically stable systems.

Table 1: Different quantum descriptive parameters of Metronidazole and Tinidazole

Compounds	**E_{HOMO}** (eV)	**E_{LUMO}** (eV)	**E_g** (eV)	**IP** (eV)	**EA** (eV)	**χ** (eV)	**μ** (eV)	**η** (eV)	**S** $(eV)^{-1}$	**ω** (eV)
Metronidazole	-7.01	-2.43	4.58	7.01	2.43	4.72	-4.72	2.29	0.44	4.86
Tinidazole	-7.13	-2.53	4.60	7.13	2.53	4.83	-4.83	2.30	0.43	5.07

Mulliken Atomic Charges

In several quantum mechanical computations, Mulliken atomic charges significantly influence the molecular structures, electronic properties, dipole moment, polarizability, and various other properties (Rijal et al., 2023). The Mulliken atomic charges of metronidazole and tinidazole drugs are expressed in Figure 5 with the plot of atoms along with their respective Mulliken charges. For both drugs, the heteroatoms, viz., oxygen and nitrogen, exhibit strong negative charges, which illustrates them as electron-rich centers that may participate in electrophilic interactions as well as hydrogen bonding.

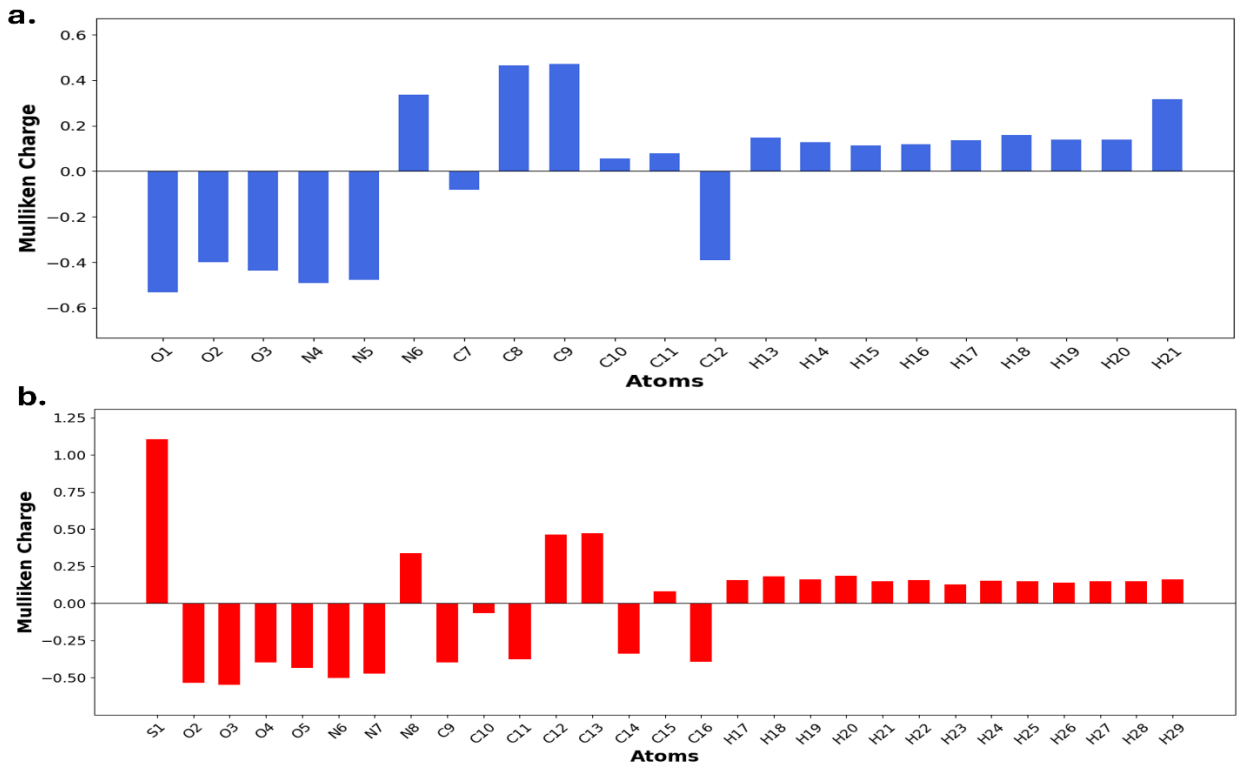

Figure 5: Mulliken Atomic Charges of (a) metronidazole and (b) tinidazole

In metronidazole, oxygen shows negative charges that range from -0.39 to -0.53, and nitrogen with negative charges ranging from -0.47 to -0.49, except for one nitrogen atom in the nitro group attached to the imidazole ring with a positive charge of +0.33. Likewise, tinidazole also shows highly negative oxygen atoms with charges ranging from -0.39 to -0.53 and nitrogen with charges ranging from -0.47 to -0.50, except for one nitrogen atom, which shows a similar positive charge of +0.33 as in metronidazole. A major difference lies in the presence of a sulphur atom in tinidazole, which carries a high positive charge of +1.10, influencing the overall electron distribution of the molecule. This positively charged sulphur in tinidazole can alter drug binding as well as interaction with biological targets compared to metronidazole. Carbon atoms and hydrogen atoms show similar charge distribution in both drugs.

MEP Surface Map Analysis

The Molecular Electrostatic Potential (MEP) map is used to understand nucleophilic and electrophilic sites, as well as weak interactions such as hydrogen bonds (Khadka et al., 2025). The different values for electrostatic potential are represented according to colored regions in the MEP map. Metronidazole exhibits a higher electrostatic potential region, plotted within the range of -0.056 a.u. to +0.056 a.u. compared to that of tinidazole plotted within the range of -0.046 a.u. to +0.046 a.u. as represented in Figure 6. The most positive electrostatic potential is indicated by blue regions, while the red region represents the most electronegative electrostatic potential, and zero electrostatic potential is symbolized by green regions (Gyawali et al., 2025).

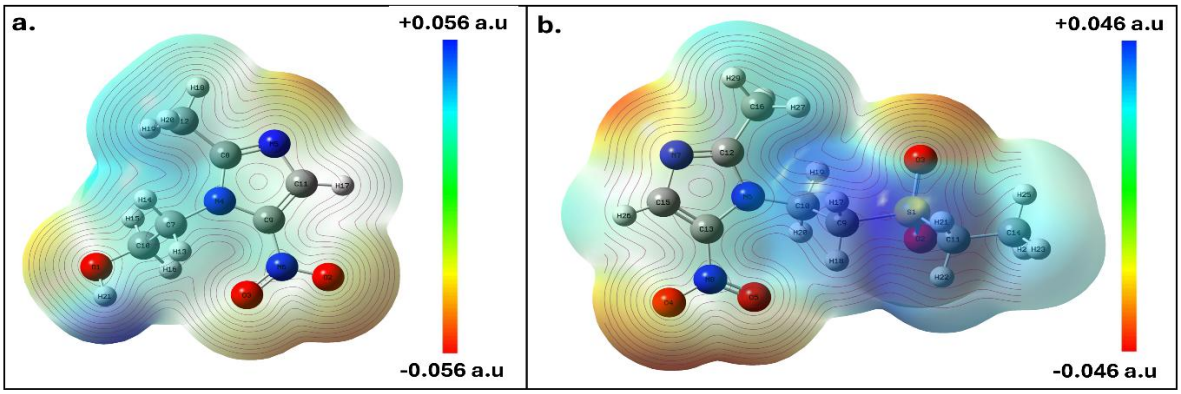

Figure 6: MEP surface map of (a) metronidazole and (b) tinidazole

In Figure 6a, metronidazole exhibits the most negative potential around the oxygen atoms, visualized by red to orange regions, suggesting sites prone to electrophilic attack. The positive regions indicated by blue regions are localized around hydrogen atoms, particularly those bonded to nitrogen and carbon atoms adjacent to the nitro group, suggesting sites prone to nucleophilic attack. Similarly, in Figure 6b, tinidazole shows a broader as well as more delocalized distribution of electrostatic potential compared to metronidazole. The regions around oxygen atoms are the most negative regions, analogous to those in metronidazole. Also, the positive regions are similarly localized around hydrogen atoms as in metronidazole, but with a lower electrostatic potential range than in metronidazole. This is probably due to the presence of a sulphur atom in the side chain that slightly alters the electrostatic regions compared to those in metronidazole.

Vibrational Analysis

Metronidazole and tinidazole have 21 and 29 atoms, respectively, which correspond to 57 and 81 possible theoretical modes of vibrations. Frequency calculations were performed after geometry optimization, confirmed by the absence of negative frequencies. The table below presents the different computed frequencies, their IR intensities, Raman activities, vibrational assignments, and corresponding potential energy distribution (PED%) contribution. The wavenumbers were scaled using 0.97 as the scaling factor, which is favoured for B3LYP/6-31 g(d,p) level (Andrade et al., 2008). Figure 7 shows the theoretical IR and Raman spectra of metronidazole and

tinidazole. From the figure, we observed that the FT-Raman spectra for the drugs metronidazole and tinidazole were almost complementary, while the FT-IR peaks in tinidazole were stronger compared to those of metronidazole, which is the result of the substituent in tinidazole, i.e., ethylsulphonylethyl side chain attached to nitroimidazole core.

- **O-H vibrations:** The O-H vibrations are typically observed within a specific frequency range of 3600-3800 cm^{-1} (Karabacak et al., 2010), where we observed it at 3701 cm^{-1} with a strong PED contribution of 100% by O1-H21 vibration in metronidazole, which is in quite good agreement.

Table 2: Vibrational analysis of metronidazole and tinidazole, along with their computed vibrational frequencies, IR intensities, Raman activities, and vibrational assignments with PED% at DFT/B3LYP(6-31G(d,p)) level

For Metronidazole

Calculated Frequency (cm-1)		IR	Raman	Vibrational Assignments
Unscaled	**Scaled**	**Intensity**	**Activity**	**[PED>10%]**
3815	3701	26.57	71.19	ν[O1-H21] (100)
3110	3017	18.94	63.63	ν[C7-H13] (90)
3048	2957	27.68	22.19	ν[C10-H15] (90)
1609	1561	195.55	7.29	ν[O2-N6] (79)
1522	1476	5.93	9.50	β[H16-C10-H15] (59), τ[H13-C7-N4-C8] (27)
1356	1315	11.22	2.42	τ[H14-C7-N4-C8] (56)
1308	1269	118.18	57.84	ν[N5-C11] (53), ν[N4-C7] (12)
1073	1041	136.36	1.46	ν[O1-C10] (44), β[H21-O1-C10] (26)
1041	1010	2.44	5.69	ν[C10-C7] (69)
894	867	7.37	2.17	τ[H17-C11-N5-C8] (85)
612	594	0.40	2.38	τ[C9-C11-N5-C8] (70)
217	211	3.39	0.50	β[C11-C9-N6] (81)
54	52	1.15	1.70	γ[C7-C8-C9-N4] (66), γ[N6-C11-N4-C9] (13)

For Tinidazole

Calculated Frequency (cm-1)		IR	Raman	Vibrational Assignments
Unscaled	**Scaled**	**Intensity**	**Activity**	**[PED>10%]**
3107	3014	6.15	66.87	ν[C16-H27] (95)
3049	2958	6.63	178.28	ν[C16-H28] (86), ν[C16-H29] (13)
1610	1562	220.71	6.71	ν[O4-N8] (77)
1501	1456	1.63	23.14	β[H28-C16-H29] (66), τ[H29-C16-C12-N6] (11)
1412	1370	164.99	49.85	ν[N7-C15] (48), β[H27-C16-H28] (31)
1309	1270	129.56	54.33	ν[N7-C12] (50), β[N6-C12-N7] (20)
1118	1084	117.50	2.75	ν[S1-O3] (73)
983	954	4.24	3.91	ν[C14-C11] (52), τ[H25-C14-C11-S1] (35)
749	727	12.18	0.78	γ[O4-C13-O5-N8] (89)
610	592	5.93	1.79	τ[C13-C15-N7-C12] (70)
362	351	1.25	1.02	γ[O2-C9-C11-S1] (60)

211	205	0.05	0.43	τ[H23-C14-C11-S1] (84), β[O2-S1-C11] (13)
104	101	1.78	0.87	τ[C9-C10-N6-C12] (58)
28	27	5.97	1.04	τ[C10-C9-S1-C11] (79)

ν = stretching mode of vibrations, β = Bending mode of vibrations, τ = Torsional mode of vibrations, γ = Out-of-plane mode of vibrations

- **C-H vibrations:** We observed the C-H vibrations at a range of 2900-3100 cm^{-1} with >90% PED contributions as mentioned in Table 2 in both drugs, which matches the 3000-3100 cm^{-1} range observed by Joshi et al. (Joshi et al., 2018).
- **O-N vibrations:** In our study, O-N vibrations were calculated at 1561 cm^{-1} in metronidazole with 79% PED contribution by O2-N6 and at 1562 cm^{-1} in tinidazole with 77% PED contribution by O4-N8. This result aligns with similar spectroscopic observations where this vibration was observed at around 1600 cm^{-1} (Harikrishnan and Bhoopathy, 2015).
- **C-N vibrations:** The C-N stretching vibrations often appear at around 1300-1000 cm^{-1} (Varsanyi, 1969; Silverstein et al., 1981). Our research showed these vibrations at 1269 cm^{-1} in metronidazole with PED contributions of 53% and 13% by N5-C11 and N4-C7, respectively, and at 1270 cm^{-1} and 1370 cm^{-1} in tinidazole with PED contributions around 50% as mentioned in Table 2.
- **Other vibrations:** The C-C vibrational frequencies were observed at around 1000 cm^{-1}, S-O vibrations at 1084 cm^{-1}, and other bending, torsional, and out-of-plane vibrations are all mentioned in Table 2 below.

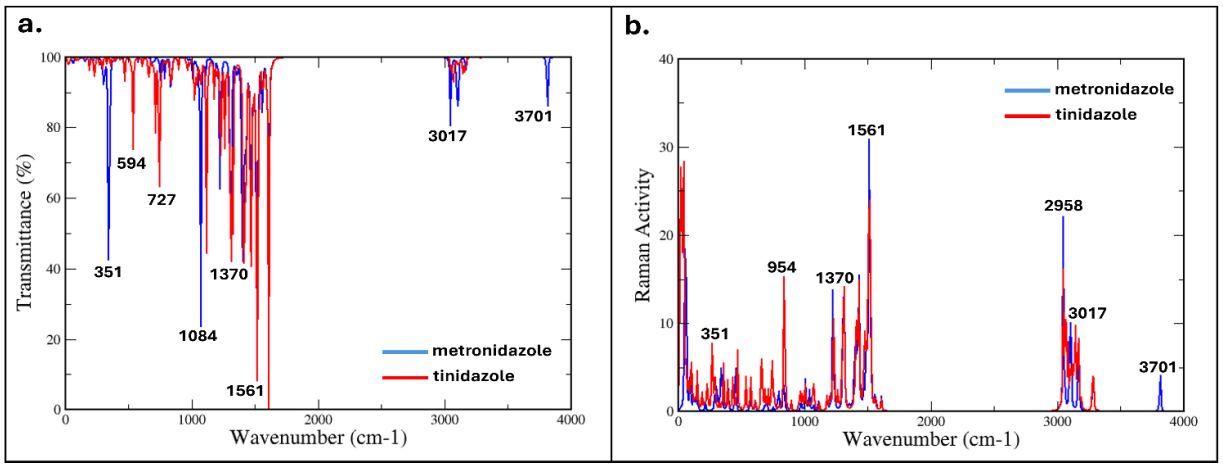

Figure 7: Theoretical spectra for metronidazole and tinidazole (a) FT-IR and (b) FT-Raman

UV-Vis Absorption Spectra Analysis

The UV-Vis spectra of metronidazole and tinidazole calculated using TD-DFT at B3LYP/6-31 G(d,p) level, are depicted in Figure 8, and the Table 3 presents the maximum wavelengths along with their corresponding excitation energies, oscillator strengths and primary orbital contributions. For metronidazole, three prominent absorption peaks were observed at 323, 292, and 287 nm. The strongest transition appears at 287 nm (f=0.1665), dominated by HOMO → LUMO excitation (85%). For

tinidazole, similar absorption features were observed at 323, 292, and 284 nm, with the strongest transition at 284 nm (f=0.2134), almost exclusively due to HOMO → LUMO transition (97%).

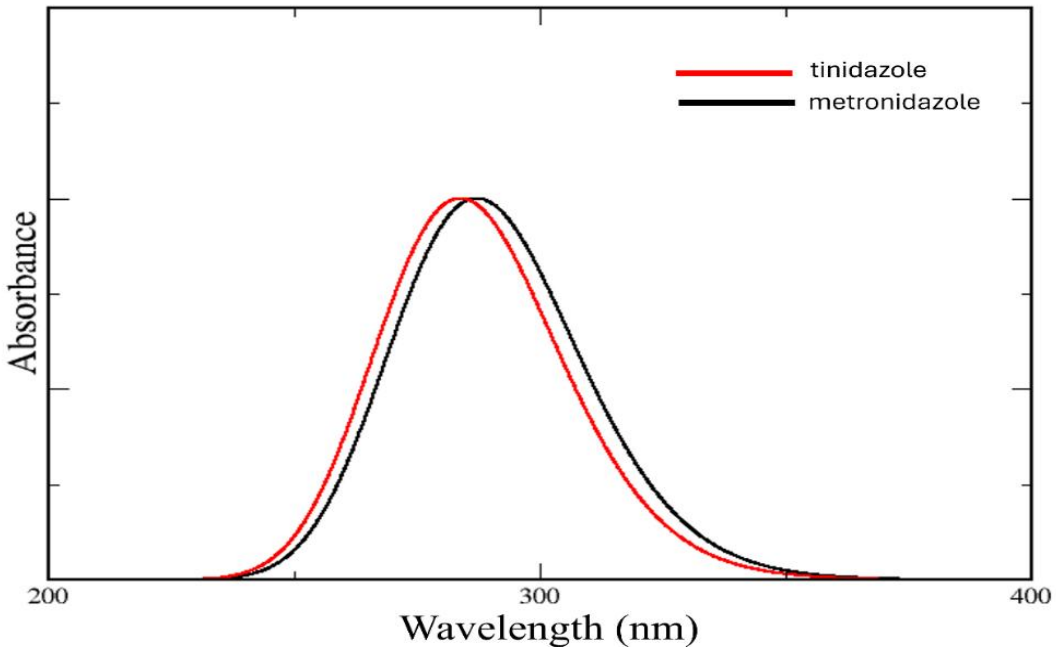

Figure 8: UV-visible absorption spectra of metronidazole and tinidazole

Both molecules exhibit strong π - π∗ transitions in the range of 280-290 nm regions, which are dominated by HOMO → LUMO transitions. However, the oscillator strength of tinidazole (f=0.2134 at 284 nm) is higher than that of metronidazole (f=0.1665 at 287 nm), which suggests stronger absorption intensity. So, the similarity in spectral patterns reflects their structural similarity, while the differences in the oscillator strengths and orbital contributions are likely caused by the influence of substituents on the electronic structure.

Table 3: Maximum wavelength along with their excitation energies, oscillator strengths and primary orbital transition contributions for UV-Vis absorption

Molecule	**Maximum Wavelength** (nm)	**Excitation Energy** (eV)	**Oscillator strength** (f)	**Major Contributions**
Metronidazole	323	3.84	0.0003	H-3 → L (45%), H-2 → L (34%), H-1 → L (19%)
	292	4.25	0.0116	H-6 → L (20%), H-3 → L (35%), H-2 → L (15%), H-1 → L (13%)
	287	4.32	0.1665	H → L (85%)
Tinidazole	323	3.84	0.0006	H-3 → L (36%), H-1 → L (56%)
	292	4.24	0.0005	H-7 → L (14%), H-3 → L (36%), H-1 → L (28%)
	284	4.37	0.2134	H → L (97%)

H= HOMO and L= LUMO

NCI-RDG Analysis

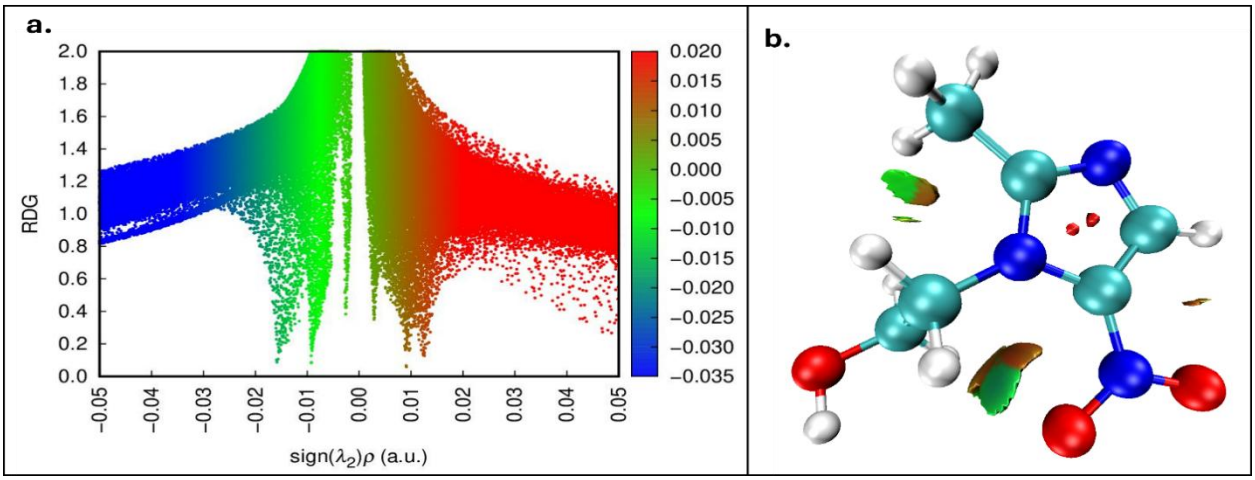

Figure 9: RDG and NCI of metronidazole (a) 2D scatter diagram and (b) 3D isosurface diagram

The Non-Covalent Interaction - Reduced Density Gradient (NCI-RDG) analysis is a method that allows researchers of quantum chemistry to explore different intermolecular interactions in depth by differentiating between the van der Waals forces, steric hindrances or repulsions, and hydrogen bonds in the title molecules under research. RDG is a basic dimensionless quantity that features weak interactions based on the quantum-mechanical electron density as well as its first derivatives in real space (Johnson et al., 2010).

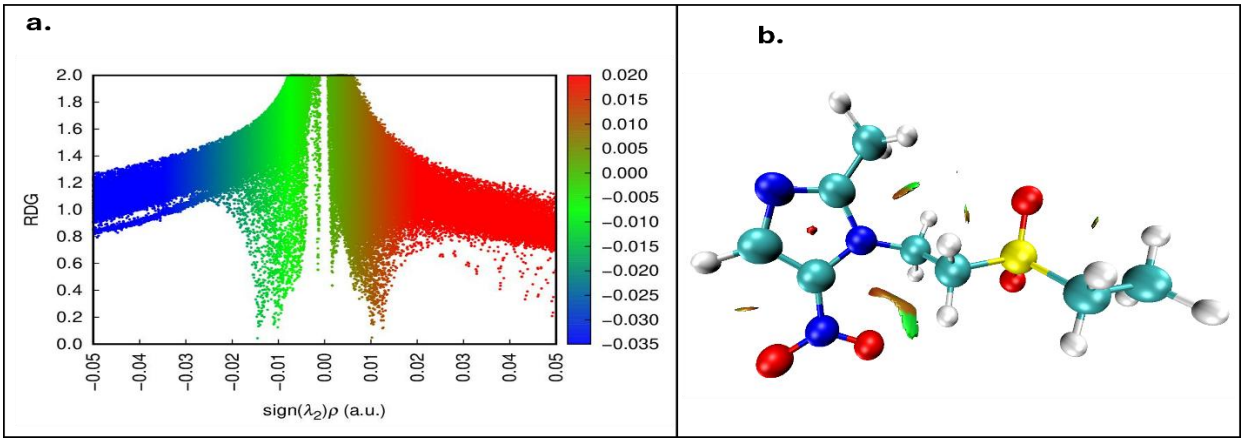

Figure 10: RDG and NCI of tinidazole (a) 2D scatter diagram and (b) 3D isosurface diagram

The NCI-RDG analysis of metronidazole and tinidazole showed both the steric repulsive effects and van der Waals forces. From Figure 9 and 10, the red spikes in the plot (for sign $(\lambda_2)\rho > 0.01$ a.u.) indicate steric repulsions, the green regions (-0.02< sign $(\lambda_2)\rho$ >.01 a.u.) correspond to weak van der Waals interactions, commonly seen

between non-bonded atoms in close convergence, the blue regions in Figure 9a and 10a (-0.05< sign (λ_2)ρ >-0.03 a.u.) signify hydrogen bonding as strong attractive interactions (Khanal et al., 2025; Boto et al., 2017). The red isosurfaces near the ring and oxygen confirm the steric repulsions, which are supposed to be typical in the case of nitroimidazole drugs. Metronidazole mainly showed localized hydrogen bonding and van der Waals interactions around the nitro group, whereas tinidazole, due to its ethylsulphonylethyl substituent, showed enhanced van der Waals interactions supported by stronger steric effects. These differences in non-covalent interaction profiles of metronidazole and tinidazole may contribute to different variations in their pharmacokinetic behaviours and biological activities.

Conclusions

In summary, we successfully computed various parameters for the two nitroimidazole-based antibiotics metronidazole and tinidazole, side-by-side. In the FMO study, tinidazole showed a slightly higher HOMO-LUMO energy gap, indicating more kinetic stability and less chemical reactivity than metronidazole, which was further validated by DOS spectra. Mulliken atomic charges and MEP surface analysis suggested oxygen atoms in both drugs were favourable for electrophilic attack, while the charge distribution was more delocalized in tinidazole compared to metronidazole and slightly different electrostatic potential regions because of the presence of an ethylsulphonylethyl substituent in tinidazole. The UV-Vis absorption spectra showed similar spectral patterns in metronidazole and tinidazole, but a stronger absorption strength in tinidazole compared to metronidazole because of a higher oscillator strength. There was an utmost similarity in the FT-Raman spectra, while the FT-IR spectra showed a slight difference, where tinidazole showed higher peaks compared to those of metronidazole. The NCI- RDG analysis visualized stronger steric repulsions and van der Waals interactions in tinidazole compared to those in metronidazole. Overall, first-principles analysis on metronidazole and tinidazole was successfully done, studying various electronic, molecular, and spectroscopic properties while getting good insights into the difference in their physicochemical properties.

References

Adhikari, D., Karki, R., Adhikari, K., & Pantha, N. (2024). First-principles study on the selective separation of toxic gases by Mg-MOF-74. ACS Omega, 9(4), 4849–4856. https://doi.org/10.1021/acsomega.3c09718

Andrade, S. G., Gonçalves, L. C. S., & Jorge, F. E. (2008). Scaling factors for fundamental vibrational frequencies and zero-point energies obtained from HF, MP2, and DFT/DZP and TZP harmonic frequencies. Journal of Molecular Structure:THEOCHEM, 864(1), 20–25. https://doi.org/10.1016/j.theochem.2008.05.025

Becke, A. D. (1993). Density-functional thermochemistry. III. The role of exact exchange. The Journal of Chemical Physics, 98(7), 5648–5652. https://doi.org/10.1063/1.464913

Ben Mahmoud, C., Anelli, A., Csányi, G., & Ceriotti, M. (2020). Learning the electronic density of states in condensed matter. Physical Review B, 102(23), 235130. https://doi.org/10.1103/PhysRevB.102.235130

Boto, R. A., Piquemal, J.-P., & Contreras-García, J. (2017). Revealing strong interactions with the reduced density gradient: A benchmark for covalent, ionic and charge-shift bonds. Theoretical Chemistry Accounts, 136(12), 139. https://doi.org/10.1007/s00214-017-2197-x

Casida, M. E. (2009). Time-dependent density-functional theory for molecules and molecular solids. Journal of Molecular Structure: THEOCHEM, 914(1–3), 3–18. https://doi.org/10.1016/j.theochem.2009.08.018

Corey, E. J. (2013). Drug discovery practices, processes, and perspectives (p. 27). Hoboken, NJ: John Wiley & Sons.

Dennington, R., Keith, T. A., & Millam, J. M. (2016). GaussView, Version 6. Shawnee Mission, KS: Semichem Inc.

Domingo, L. R., Ríos-Gutiérrez, M., & Pérez, P. (2016). Applications of the conceptual density functional theory indices to organic chemistry reactivity. Molecules, 21(6), 748. https://doi.org/10.3390/molecules21060748

Ebel, K., Koehler, H., Gamer, A. O., & Jäckh, R. (2002). Imidazole and derivatives. In Ullmann's Encyclopedia of Industrial Chemistry. https://doi.org/10.1002/14356007.a13_661

Frisch, M. J., Trucks, G. W., Schlegel, H. B., Scuseria, G. E., Robb, M. A., Cheeseman, J. R., & al., E. (2016). Gaussian 16, Revision C.01. Wallingford, CT: Gaussian, Inc.

Geerlings, P., De Proft, F., & Langenaeker, W. (2003). Conceptual density functional theory. Chemical Reviews, 103(5), 1793–1874. https://doi.org/10.1021/cr990029p

Gyawali, K., Chhetri, S. P., Khanal, K., Kshetri, M. B., Maharjan, R., Acharya, A., … Lamichhane, T. R. (2025). Inhibition potential of quercetin similar compounds to SARS-CoV-2 main protease by high-throughput virtual screening, molecular simulations, ADMET analysis, and DFT studies. Chemistry & Biodiversity, 22(e01485). https://doi.org/10.1002/cbdv.202501485

Harikrishnan, S., & Bhoopathy, T. J. (2015). Density functional theory, restricted Hartree-Fock simulations and FTIR, FT-Raman and UV-Vis spectroscopic studies on metronidazole. International Journal of ChemTech Research, 7(1), 460–473.

He, S., Yin, R., Lai, T., Zhao, Y., Guo, W., & Zhu, M. (2021). Structure-dependent degradation of nitroimidazoles by cobalt–manganese layered double hydroxide catalyzed peroxymonosulfate process. Chemosphere, 266, 129006. https://doi.org/10.1016/j.chemosphere.2020.129006

Humphrey, W., Dalke, A., & Schulten, K. (1996). VMD – Visual molecular dynamics. Journal of Molecular Graphics, 14(1), 33–38. http://www.ks.uiuc.edu/Research/vmd/

Jenks, P. J. (2010). Nitroimidazoles. In R. G. Finch, D. Greenwood, S. R. Norrby, & R. J. Whitley (Eds.), Antibiotic and chemotherapy (9th ed., pp. 292–300). https://doi.org/10.1016/b978-0-7020-4064-1.00024-5

Johnson, E. R., Keinan, S., Mori-Sánchez, P., Contreras-García, J., Cohen, A. J., & Yang, W. (2010). Revealing noncovalent interactions. Journal of the American Chemical Society, 132(18), 6498–6506. https://doi.org/10.1021/ja100936w

Joshi, B. D., Srivastava, A., Tondon, P., Jain, S., & Ayla, A. (2018). A combined experimental (IR, Raman and UV-Vis) and quantum chemical study of canadine. Spectrochimica Acta Part A: Molecular and Biomolecular Spectroscopy, 199, 249–258. https://doi.org/10.1016/j.saa.2018.01.055

Karabacak, M., Cinar, M., Unal, Z., & Kurt, M. (2010). FT-IR, UV spectroscopic and DFT quantum chemical study on the molecular conformation, vibrational and electronic transitions of 2-aminoterephthalic acid. Journal of Molecular Structure, 982(1–3), 22–27. https://doi.org/10.1016/j.molstruc.2010.07.033

Khadka, M., Sah, M., Chaudhary, R., & Others. (2025). Spectroscopic, quantum chemical, and topological calculations of the phenylephrine molecule using density functional theory. Scientific Reports, 15, 208. https://doi.org/10.1038/s41598-024-81633-2

Khanal, K., Chhetri, M. B., Khanal, M., Acharya, A., Maharjan, R., Gyawali, K., … Lamichhane, T. R. (2025). DFT analysis on electronic properties, reactivity and adsorption mechanism of Favipiravir/XTiO4H2 (X = Pt, Zr, Zn) nanocomplexes and their biological evaluations. Trends in Sciences, 22(9), 10384–10384. https://doi.org/10.31557/TiS.2025.22.9.10384

Koopmans, T. (1934). Über die Zuordnung von Wellenfunktionen und Eigenwerten zu den einzelnen Elektronen eines Atoms. Physica, 1, 104–113. https://doi.org/10.1016/S0031-8914(34)90011-2

Lee, C., Yang, W., & Parr, R. G. (1988). Development of the Colle–Salvetti correlation-energy formula into a functional of the electron density. Physical Review B, 37(2), 785. https://doi.org/10.1103/PhysRevB.37.785

Lu, T., & Chen, F. (2012). Multiwfn: A multifunctional wavefunction analyzer. Journal of Computational Chemistry, 33(5), 580–592. https://doi.org/10.1002/jcc.22885

Mital, A. (2009). Synthetic nitroimidazoles: Biological activities and mutagenicity relationships. Scientia Pharmaceutica, 77(3), 497–520. https://doi.org/10.3797/scipharm.0907-14

Mulliken, R. S. (1955). Electronic population analysis on LCAO–MO molecular wave functions. I. The Journal of Chemical Physics, 23(10), 1833–1840. https://doi.org/10.1063/1.1740588

O'Boyle, N. M., Tenderholt, A. L., & Langner, K. M. (2008). Cclib: A library for package-independent computational chemistry algorithms. Journal of Computational Chemistry, 29(5), 839–845. https://doi.org/10.1002/jcc.20823

Padmanabhan, J., Parthasarathi, R., Subramanian, V., & Chattaraj, P. K. (2007). Electrophilicity-based charge transfer descriptor. The Journal of Physical Chemistry A, 111(7), 1358–1361. https://doi.org/10.1021/jp0654464

Pandey, B. K., Pandey, S. K., & Pandey, D. (2011). A survey of bioinformatics applications on parallel architectures. International Journal of Computer Applications, 23(4), 21–25. https://doi.org/10.5120/2866-3800

Pearson, R. G. (1989). Absolute electronegativity and hardness: Applications to organic chemistry. Journal of Organic Chemistry, 54(6), 1423–1430. https://doi.org/10.1021/jo00267a034

Rijal, R., Sah, M., & Lamichhane, H. P. (2023). Molecular simulation, vibrational spectroscopy and global reactivity descriptors of pseudoephedrine molecule in different phases and states. Heliyon, 9(3), e14801. https://doi.org/10.1016/j.heliyon.2023.e14801

Schwebke, J. R., & Desmond, R. A. (2011). Tinidazole vs metronidazole for the treatment of bacterial vaginosis. American Journal of Obstetrics and Gynecology, 204(3), 211.e1. https://doi.org/10.1016/j.ajog.2010.10.898

Shi, S., Yu, H., Yang, F., Yao, W., & Xie, Y. (2022). Simultaneous determination of 14 nitroimidazoles using thin-layer chromatography combined with surface-enhanced Raman spectroscopy (TLC-SERS). Food Bioscience, 48, 101755. https://doi.org/10.1016/j.fbio.2022.101755

Silverstein, M., Basseler, G. C., & Morill, C. (1981). Spectrometric identification of organic compounds. New York, NY: Wiley.

Trivedi, M. K., Patil, S., Shettigar, H., Bairwa, K., & Jana, S. (2015). Spectroscopic characterization of biofield treated metronidazole and tinidazole. Medicinal Chemistry, 5(7), 340–344.

Varsanyi, G. (1969). Vibrational spectra of benzene derivatives. New York, NY: Academic Press.